

Article

Coating on Steel Discs with a Photocatalytic System CuO/SiO₂ for the Degradation of the Ubiquitous Contaminants Methylene Blue and Amoxicillin

Alberto Hernández-Reyes ¹, Irina V. Lijanova ^{1,*} , Aristeo Garrido-Hernández ², Ángel de J. Morales-Ramírez ¹, Carlos Hernández-Fuentes ^{1,3}, Evelyn Y. Calvillo-Muñoz ⁴ , Natalya V. Likhanova ⁴  and Octavio Olivares-Xometl ⁵ 

- ¹ Centro de Investigación e Innovación Tecnológica, Instituto Politécnico Nacional, Ciudad de México 02250, Mexico; alberto.hernandez.r011@gmail.com (A.H.-R.); angel_ipn77@hotmail.com (Á.d.J.M.-R.); charlos_552@hotmail.com (C.H.-F.)
 - ² División Químico Biológicas, Universidad Tecnológica de Tecámac, Tecámac, Estado de México 55740, Mexico; agarridoh@uttecamac.edu.mx
 - ³ Escuela Superior de Ingeniería Mecánica y Eléctrica, Instituto Politécnico Nacional, Av. Luis Enrique Erro S/N, Unidad Profesional Adolfo López Mateos, Zacatenco, Delegación Gustavo A. Madero, Ciudad de México 07738, Mexico
 - ⁴ Instituto Mexicano del Petróleo, Eje Central Norte Lázaro Cárdenas No. 152, Col. San Bartolo Atepehuacan, G. A. Madero, Ciudad de México 07730, Mexico; evelyndi.yarelyos@gmail.com (E.Y.C.-M.); nvictoro@imp.mx (N.V.L.)
 - ⁵ Facultad de Ingeniería Química, Benemérita Universidad Autónoma de Puebla, Av. San Claudio y 18 Sur, Ciudad Universitaria, Col. San Manuel, Puebla 72570, Mexico; oxoctavio@yahoo.com.mx
- * Correspondence: irinalijanova@yahoo.com.mx



Citation: Hernández-Reyes, A.; Lijanova, I.V.; Garrido-Hernández, A.; Morales-Ramírez, Á.d.J.; Hernández-Fuentes, C.; Calvillo-Muñoz, E.Y.; Likhanova, N.V.; Olivares-Xometl, O. Coating on Steel Discs with a Photocatalytic System CuO/SiO₂ for the Degradation of the Ubiquitous Contaminants Methylene Blue and Amoxicillin. *Coatings* **2024**, *14*, 523. <https://doi.org/10.3390/coatings14050523>

Academic Editor: Carlos Jose Macedo Tavares

Received: 24 March 2024
Revised: 19 April 2024
Accepted: 22 April 2024
Published: 24 April 2024



Copyright: © 2024 by the authors. Licensee MDPI, Basel, Switzerland. This article is an open access article distributed under the terms and conditions of the Creative Commons Attribution (CC BY) license (<https://creativecommons.org/licenses/by/4.0/>).

Abstract: The present research work describes the synthesis and characterization of CuO/SiO₂ for coating-perforated 304 stainless steel (SS) substrates to degrade methylene blue and amoxicillin under visible light irradiation. The foregoing photocatalytic system was achieved through the coprecipitation method by adding pure CuO to a SiO₂ sol at 1:5, 1:10, and 1:15 molar ratios. The conditions for carrying out the depositions on the SS substrates (three per substrate) involved an immersion rate of 90 mm/min with a drying time of 20 min at 120 °C. The XRD technique confirmed the presence of the SiO₂ amorphous phases and CuO monoclinic systems in the coatings, with a particle size distribution ranging from 0.5 to 2.5 μm (with an average of 1.26 ± 0.06 μm). As for SEM, it revealed a homogeneous coating surface without cracks. The produced photoactive CuO/SiO₂ coatings were capable of degrading methylene blue (98%) at 1500 min and amoxicillin (55%) at 450 min.

Keywords: coatings with a CuO:SiO₂ system; photocatalysis; emerging contaminants

1. Introduction

The main organic derivatives present in water effluents, in most cases, are anthropogenic contaminants (ACs), which are residues coming from agricultural activities, the food industry, drugs, personal care products, and medicaments [1]. These ACs have been identified as capable of provoking hormonal imbalances in living beings that manifest in metabolism, neurological, immune, and reproductive system disorders [2]. A high percentage (60%–90%) of antibiotics are not metabolized by living beings, and their excretions are released into the sewer system; unfortunately, even marine fauna are affected by the presence of pharmaceutical products such as amoxicillin and ciprofloxacin in the sea [3–5]. In addition to the foregoing molecules, the popular aromatic-structured dye methylene blue (MB), which has been reported as an environmentally persistent, toxic, carcinogenic, and mutagenic substance [6], has also been found in different aqueous media. Wastewater treatment plants are not totally efficient in eliminating these kinds of

chemicals, thus contributing to the persistence of pharmaceuticals in water and the growth of antibiotic-resistant microorganisms [7]. The study, development, and application of advanced materials in water remediation have attracted special interest in recent years, focusing on the use of novel technologies for the degradation and effective separation of ACs from water. Currently, membrane filtration is found among the employed physicochemical processes and is one of the studied technologies for the separation of pharmaceuticals, although it features important limitations such as fast saturation and the implementation of subsequent stages of waste separation, increasing the number of unit operations in the process, which considerably reduces its efficiency [8–11]. Another alternative is represented by porous materials such as activated carbon, silica, and zeolites, which, by means of the adsorption phenomenon, solve the saturation problems, although more studies on effective desorption mechanisms are required [12–14]. Recently, the advanced oxidation processes (AOPs), which include ozonization, the Fenton process, and photocatalysis, have become an alternative for the transformation of organic compounds whose main attractive feature is their high reactivity, which significantly shortens the degradation times [15]. As for photocatalysis, it has drawn particular interest as it employs solar light as its main energy source, and it has proven its capacity to degrade different pharmaceuticals such as cefalexin, arbidol hydrochloride, ibuprofen, and amoxicillin [16–19]. Such efficiency is based on the degradation ability through free radicals like $\bullet\text{OH}$ and $\bullet\text{O}_2^-$ derived from the production of electron-hole pairs (e^+/h^-) resulting from the interaction between a semiconductor material (photocatalyst) and aqueous medium [20]. In this context, CuO is a versatile photocatalyst due to unique characteristics like a narrow band gap (E_g), which ranges from 1.22 to 1.9 eV [21], allowing for a higher charge transfer rate, and its abundance and low-cost material; such features can be enhanced by different strategies like doping [22], the generation of crystalline framework defects [23], and the synthesis of materials consisting of two or more semiconductors [24]. In order to improve CuO dispersion and boost its photocatalytic properties, silica has been considered a suitable support material due to its thermal, electronic, and catalytic properties [25]. The combined properties of CuO and SiO₂, where they are shaped as porous spheres, have stood out in the application as detectors of organic substances of interest in the food industry [26]; also, the antimicrobial and antifungal features of CuO and SiO₂ have been utilized in construction materials [27]. The preparation methods of CuO/SiO₂ catalysts depend on their application; for example, through the sol–gel method, it is possible to support a photocatalytic material on a stable SiO₂ vitreous matrix. This methodology has been used to prepare photocatalysts featuring the CuO/SiO₂ system, which have achieved degrading percentages above 90% of contaminants such as rhodamine B [28], methylene blue, and metronidazole [29].

The degradation of pharmaceuticals like amoxicillin through photocatalytic methods has been widely studied; one of the techniques that stands out is the use of adsorbent materials (like activated carbon) along with a photocatalyst (CuO), which was able to increase the removal of amoxicillin at concentrations of up to 100 ppm from 68% to 98% [20]. As for photocatalyst disposal, it has been shown that the use of powders requires further separation stages of the active material. For this reason, the synthesis of immobilized photocatalysts represents a practical alternative [30]. To this end, 304 stainless steel has been used as a substrate for the deposition of SiO₂ films [31,32].

In the present research work, a synthesis route was proposed to obtain the photocatalytic system CuO/SiO₂ deposited on SS. The CuO bandgap was calculated, and the compositional characterization of CuO and CuO/SiO₂ was carried out using FTIR spectroscopy. The structural characterizations were carried out using X-ray diffraction (XRD), and the morphological characterizations were performed using scanning electron microscopy (SEM). Finally, the use of a CuO photocatalyst embedded in a SiO₂ matrix was proposed to evaluate the degradation efficiency of methylene blue (MB) and amoxicillin (AMX) in an aerated and stirred tank.

2. Materials and Methods

2.1. Synthesis of CuO Powders

CuO was synthesized using the coprecipitation method. First, 700 mL of 1 M ascorbic acid (Meyer, Ciudad de México, Mexico) was mixed with 700 mL of a 0.2 M solution of copper (II) acetate (Sigma, Ciudad de México, Mexico); the mixture was kept under continuous stirring for 20 h at 80 °C. Afterward, the solution was left to age for 20 days. Following this period, CuO was separated from the solution through centrifugation, and the CuO suspension was dried at 120 °C for 4 h to produce powdered CuO. Finally, the obtained powders were treated thermally at 400 °C for 4 h. The synthesized CuO was characterized using UV-Vis Perkin Elmer model Lambda 35 UV-vis spectrophotometer (PerkinElmer, Waltham, MA, USA), XRD D8 Advance diffractometer (Bruker, Karlsruhe, Germany), FTIR (Nicolet 8700, Madison, WI, USA) and SEM HITACHI TM3030 (Hitachi High-Tech, Tokyo, Japan) techniques.

2.2. Synthesis of the SiO₂ Sol

For the synthesis of 10 mL of the SiO₂ sol, first, tetraethyl orthosilicate (TEOS) (Sigma Aldrich, St. Louis, MI, USA, 97%), bidistilled water and ethanol (Meyer, Ciudad de México, Mexico) were mixed. The molar ratios of ethanol to TEOS and of water to TEOS were 4:1 and 11.67:1, respectively. Afterward, to catalyze the hydrolysis/condensation reaction, 0.034 mol of HCl (Meyer, Ciudad de México, Mexico) was added per 1 mol of TEOS. The solution was kept under continuous stirring for 3 h at 40 °C.

2.3. Deposition and Characterization of the CuO/SiO₂ Films via Dip Coating

Three theoretical CuO:SiO₂ molar ratios (1:5, 1:10, and 1:15) were studied. For the deposition step, the previously synthesized pure CuO was used, which was added to 20 mL of the SiO₂ sol for each molar ratio. Substrates of perforated 304 stainless steel were employed, which underwent an abrading treatment with a grinder. The average size of the rectangular substrates of the 304 stainless steel was 5 cm × 1.5 cm with a thickness of 0.1 cm. The depositions were carried out at an immersion rate of 90 mm/min with a drying time of 20 min at 120 °C. After finishing the depositions, the films were subjected to a curing treatment in a muffle at 600 °C for 4 h. Three depositions were performed per substrate.

For the characterization of the CuO/SiO₂ system via XRD and FTIR, the sol powders at the three molar ratios (1:5, 1:10, and 1:15) of CuO:SiO₂ were used. In order to carry out the SEM analysis, 304 stainless steel substrates (1 cm × 1 cm) were prepared simultaneously.

2.4. Characterization

To determine the crystalline structure and phase of the pure compounds of CuO, SiO₂, and the CuO/SiO₂ system at the molar ratios 1:5, 1:10, and 1:15, a Bruker eco D8 Advance diffractometer (Bruker, Karlsruhe city, Germany) using Cu-K α radiation was employed. The samples were analyzed at 25 °C in the 2 θ angle range of 4° to 80° with a step of 0.02 s⁻¹. The surface morphological analysis of the coatings at the three molar ratios of CuO/SiO₂ (1:5, 1:10, and 1:15) was carried out using a HITACHI TM3030 (Hitachi High-Tech, Tokyo, Japan) Table Top scanning electron microscope coupled with EDS. A Perkin Elmer Spectrum 65 spectrophotometer (PerkinElmer, Waltham, MA, USA) with a scan of 400 to 4000 cm⁻¹ was used for the compositional analysis of the pure CuO and SiO₂ powders, as well as the three CuO/SiO₂ systems. For the MB and AMX degradation tests, a Perkin Elmer Lambda 35 spectrophotometer (PerkinElmer, Waltham, MA, USA) was employed, scanning from 200 to 800 nm. The determination of the bandgap of CuO was conducted using the same equipment, analyzing a sample of CuO powder. With the obtained absorbance data, the Tauc equation was utilized to relate the absorption coefficient to the energy of incident radiation and E_g.

2.5. Evaluation of the Photocatalytic Efficiency of CuO Powders at Different Loadings

In order to compare the use of powders in solution versus that of the coatings, different amounts of CuO were evaluated in the degradation of MB. Initially, 180 mL of bidistilled water and MB (Meyer, Ciudad de México, Mexico) at 10 ppm were mixed in a beaker with continuous stirring. Four visible-light lamps (4.5 watts and 400 lm Phillips® model MR16, Ciudad de México, Mexico) were installed. The arrangement of the lamps and the solution can be seen in Figure 1, with the irradiance of the light sources also indicated. All photocatalytic tests were carried out inside a dark box.

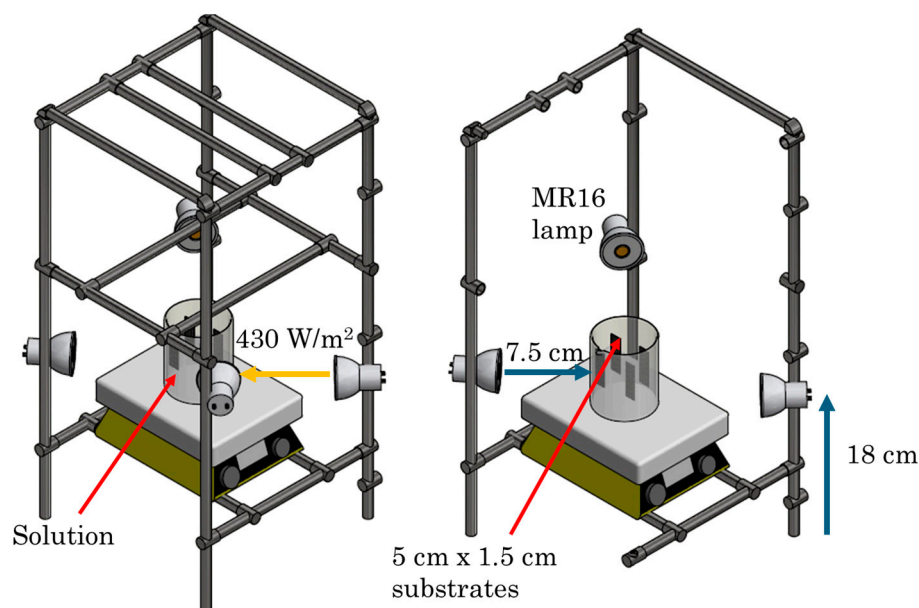


Figure 1. Arrangement of the substrates inside the dark box; the distance of the lamps and irradiance levels are specified. The irradiance was tested in a straight line to the lamp in the distance between the tank and light source. The lamps were placed in a radial arrangement in order to guarantee the illumination of the container circumference.

The degradation of MB at 10 ppm was tested using three different MB:CuO molar ratios (1:1, 1:10, and 1:100). The degradation level of each cycle was measured every 20 min using UV-Vis. To separate the powders from the MB solution, the sample was centrifuged for 10 min at 4500 rpm. Additionally, a test was conducted using CuO/SiO₂ films at a molar ratio of 1:10. The use of CuO powders changed for 4 substrates coated with the CuO/SiO₂ system, which were immersed in the solution horizontally. The substrate arrangement can be seen in Figure 1.

2.6. Photocatalytic Evaluation of the CuO/SiO₂ Films

In this first part, the best CuO:SiO₂ molar ratio for the coatings was determined in order to carry out the evaluation in the reactor with MB and AMX. For each assay, 180 mL of double-distilled water and MB (5 ppm) or AMX (10 ppm) were first mixed in a beaker. The reduction of the MB concentration was intended to improve the monitoring of the degradation curve. The same experimental arrangement was used with the CuO powders. The main variation lay in immersing 4 substrates coated with the films, replacing the use of powders, as seen in Figure 1. Three CuO:SiO₂ molar ratios (1:5, 1:10, and 1:15) were evaluated. Intervals of 30 min were employed for maximal monitoring of 9 h.

2.7. The CuO/SiO₂ System in an Aerated and Stirred Tank

In order to evaluate the CuO/SiO₂ films in an aerated and stirred tank, initially, 1.8 L of distilled water and either MB (5 ppm) or AMX (10 ppm) were mixed in the reactor tank. The same arrangement of 4 lamps (4.5 W) was employed. Additionally, to increase the

power, a 100-W lamp (100 W Tianlai[®] model R28W100, Ciudad de México, Mexico) was added. Figure 2 specifies the arrangement and the level of irradiance emitted by the lamps. A mechanical stirrer (JJ-1 Precise Strength Power Mixer VEVO[®], Zhejiang, China) and an air pump (SUNNY aquarium[®] model SAP-300, Estado de México, México) with a flow rate of 1.5 L/min were used. The reactor was made of borosilicate with a maximal capacity of 2 L and space for 4 circular substrates with a diameter of 10.7 cm. To start the operation, the 4 circular substrates coated with the CuO/SiO₂ system were placed inside the reactor. The degradation level of each cycle was monitored every 30 min.

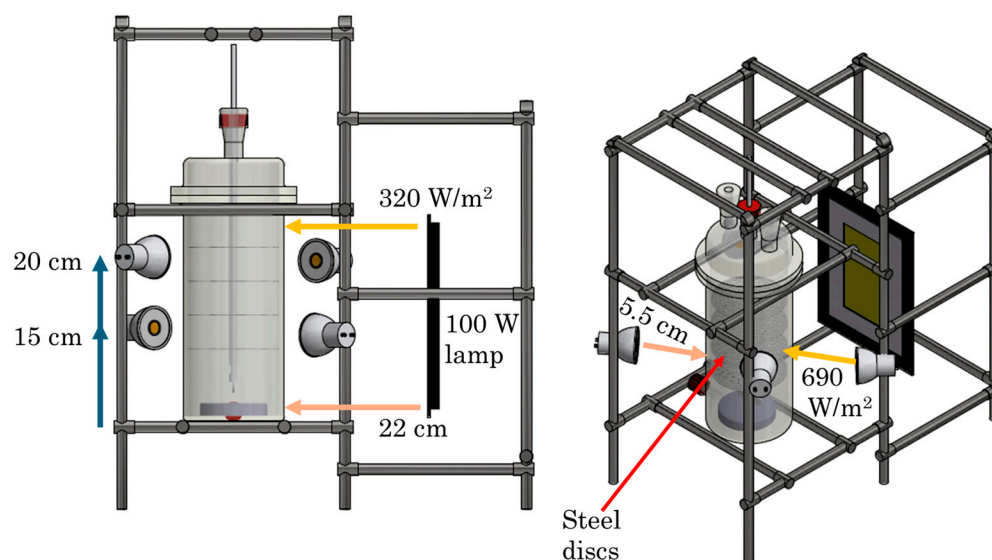


Figure 2. Description of the lamp arrangement used in the aerated and stirred tank reactor. The distance and irradiance level are specified. The irradiance was tested in a straight line with the lamp in the distance between the tank and the light source.

3. Results and Discussion

In order to establish the morphological and structural characteristics of CuO, we first conducted the characterization of the CuO powders using UV–Vis, SEM, XRD, and FTIR. Afterward, we characterized the films of the CuO/SiO₂ system using XRD and FTIR to observe the crystalline phases and chemical bonds present at the three molar ratios in comparison with the pure materials. SEM allowed for the identification of the morphological characteristics of the CuO/SiO₂ deposits. Finally, we evaluated the degradation efficiency of MB and AMX in 180 mL volumes and in the reactor (1.8 L).

3.1. Characterization of the CuO Powders

3.1.1. Ultraviolet–Visible (UV–Vis) Spectroscopy

Figure 3 (on the left) shows the UV–Vis spectrum of CuO. Two absorption bands at 223 and 274 nm are displayed. The absorbance increase from 300 nm reveals the capacity of the material to absorb material within the visible spectrum (from 400 to 700 nm).

Through the Tauc graphical method, the absorbance values of the UV–Vis plot were transformed in order to establish the width of the band gap (E_g) of the synthesized CuO, based on approximating the straight line section with the x -axis, where the intersection point represents the order of E_g . Figure 3, on the right, shows the approximation achieved using this method. The common E_g value for CuO ranges from 1.0 to 1.9 eV [33], and the obtained value for the analyzed sample was 1.86 ± 0.08 eV (the standard error was derived from the in-triplicate calculation of the E_g with the same method). Band-gap widths with present values was susceptible to visible light.

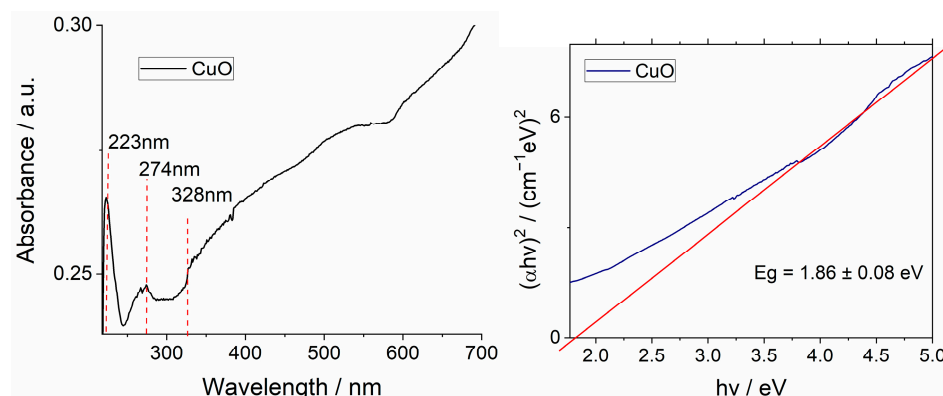


Figure 3. Absorbance spectrum (UV–Vis) of CuO synthesized via coprecipitation (**on the left**). Tauc plot for measuring the E_g of CuO (**on the right**).

3.1.2. Scanning Electron Microscopy (SEM)

By means of SEM, it is possible to observe the dispersion of clusters on the micron scale (Figure 4, on the left). The 7000 \times magnification reveals the polyhedral morphology of the CuO microcrystals.

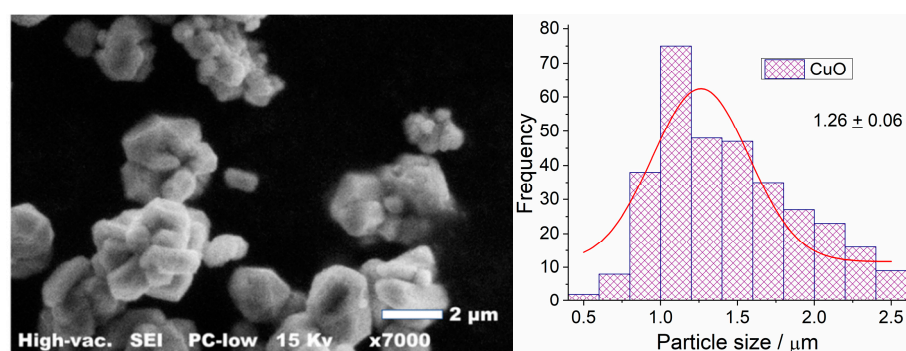


Figure 4. SEM of the CuO powders synthesized via coprecipitation at 7000 \times (**on the left**) and particle size analysis, obtained by analyzing 300 particles from different sections with the ImageJ 1.54d program (**on the right**).

Using particle size analysis (Figure 4, on the right), we found a size distribution ranging from 0.5 to 2.5 μm with an average microcrystal size of $1.26 \pm 0.06 \mu\text{m}$. The coprecipitation method proved effective in forming particles with a homogeneous shape and polyhedral morphology with flat faces. A similar morphology was reported by Nogueira et al. [29] whose material achieved 98% efficiency in degrading MB.

3.2. Characterization of the CuO/SiO₂ Films

3.2.1. X-ray Diffraction

Figure 5 shows the comparison of the diffractograms for the different systems synthesized at different molar ratios (1:5, 1:10, and 1:15) of CuO:SiO₂.

The diffractogram corresponding to SiO₂ using the sol–gel methodology displays a band formed between 15° and 30°, which confirms the SiO₂ amorphous phase. Furthermore, the absence of high-intensity narrow peaks corresponding to quartz or cristobalite, which appear at 26.19° (ICSD-98-000-9482) and 21.47° (ICSD-98-002-4587), respectively, rules out the formation of secondary phases. The reference crystallographic card ICDD-03-065-2309 belongs to the CuO monoclinic system. The comparison reveals the presence of peaks that are characteristic of the foregoing phase.

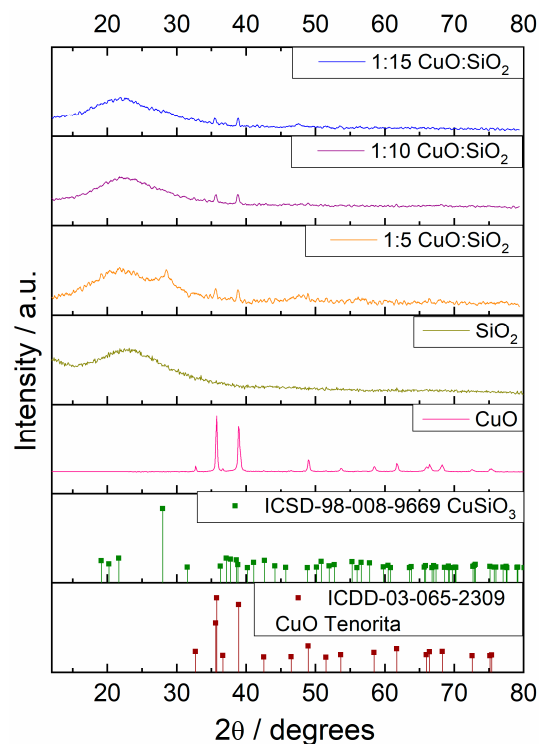


Figure 5. XRD diffractograms of CuO (using the coprecipitation method) and pure SiO₂ (using the sol-gel method) in comparison with those corresponding to the CuO/SiO₂ systems at different molar ratios (1:5, 1:10, and 1:15).

The well-defined, high-intensity peaks of CuO confirm the crystallization of the material. A crystallized material promotes the transport of charges, thus directly affecting its photocatalytic properties [34]. The diffractograms of the systems with 1:5 and 1:10 molar ratios show two peaks at 35.55° and 38.75° that are characteristic of the CuO monoclinic phase, which are visibly lower for the 1:15 molar ratio. This fact is due to the diminution of the CuO charge. For the systems with the 1:10 and 1:15 molar ratios, the formation of compounds different from amorphous SiO₂ or monoclinic CuO was not observed. Notwithstanding, for the 1:5 molar ratio, the presence of a wide peak between 25° and 30° is associated with the possible formation of copper silicates derived from the CuO concentration increase. Chen et al. [35] reported that the formation of copper silicate in solution is possible. In their study, the authors started from Cu(NO₃)₂ to form a blue-green Cu(OH)₂ precipitate, which was put in contact with an alkaline silicate solution in order to carry out a hydrothermal process that allowed the formation of porous copper silicates. In addition, Guoqin Cao et al. elucidated the formation of a nanostructured coating system with Si, diversifying the requirement for a “structure-performance relationship”, where the depressed Si inner-diffusion led to the formation of an amorphous bilayer structure [36,37]. In this work, it was also mentioned that other synthesis approaches, such as sol-gel or coprecipitation, can be employed.

3.2.2. Fourier Transform Infrared (FTIR) Spectroscopy

Figure 6 shows a comparison of the FTIR spectra corresponding to the CuO and SiO₂ powders using the sol-gel and coprecipitation methods. Additionally, the three CuO/SiO₂ systems at the three proposed molar ratios (1:5, 1:10, and 1:15) are also compared.

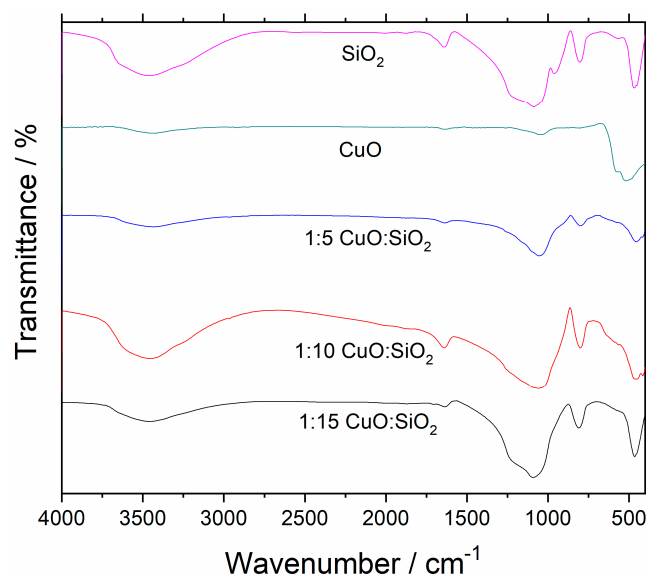


Figure 6. FTIR spectra of pure SiO_2 powders using the sol-gel method and CuO using the coprecipitation method. The FT-IR spectra of the CuO/ SiO_2 systems at molar ratios of 1:5, 1:10, and 1:15 are recorded from powder samples of the sols at 600°C .

In the spectrum corresponding to pure SiO_2 , an intense band between 1000 and 1300 cm^{-1} , which is characteristic of the asymmetric stretching of the Si-O bond, was observed. The signal at 957 cm^{-1} belongs to the Si-OH bond, coming from the surface functionalization of SiO_2 , characteristic of SiO_2 via the sol-gel route [38]. As for the band at 800 cm^{-1} , it is ascribed to the symmetric stretching vibrations of the Si-O-Si bonds. The bending O-Si-O vibrations are represented by a middle intensity band between 400 and 500 cm^{-1} [39]. The different vibrational modes of the Cu-O bond occur between 400 and 800 cm^{-1} [40]. The most intense band at 516 cm^{-1} and 1047 cm^{-1} is associated with the bending vibrations of the Cu-O bond. A weak band at 1631 cm^{-1} is derived from the stretching vibration of the Cu-O bond [41]. At 3421 cm^{-1} , a characteristic band of the O-H bond, stemming from water present in the environment and adsorbed by CuO, becomes visible. For the CuO/ SiO_2 system at a 1:5 molar ratio, bands from the different vibrations of the Si-O bond in SiO_2 are observed. This system contains the highest amount of CuO, but due to the fact that the vibrations of the Si-O and Cu-O bonds occur in the same region, the characteristic CuO band overlaps those of SiO_2 . Likewise, the concentration is a function of the material absorption, and in the CuO/ SiO_2 system, CuO has the lowest concentration of the three proposed molar ratios. For this reason, in the systems with the 1:15 and 1:10 molar ratios, the characteristic SiO_2 bands are more evident.

The 1:10 molar ratio of the powdered CuO/ SiO_2 system displays a more intense band between 3250 cm^{-1} and 3750 cm^{-1} , which indicates the presence of a more hydrophilic compound with good adsorption capacity [38]. This fact benefits the system's capacity to generate intermolecular interactions with the contaminants.

3.2.3. Scanning Electron Microscopy (SEM)

In order to analyze the morphology of the CuO/ SiO_2 films, we employed the SEM technique. Figure 7a shows the micrograph of the CuO/ SiO_2 system films at a 1:5 molar ratio and $40\times$ magnification. The distribution of the CuO/ SiO_2 system deposited on a sample of the 304 stainless steel substrates can be observed. The thermal treatments affect the topography of the films, e.g., at $2000\times$ magnification (Figure 7b), where the cracking of the film layers is evident due to the treatment process at 600°C .

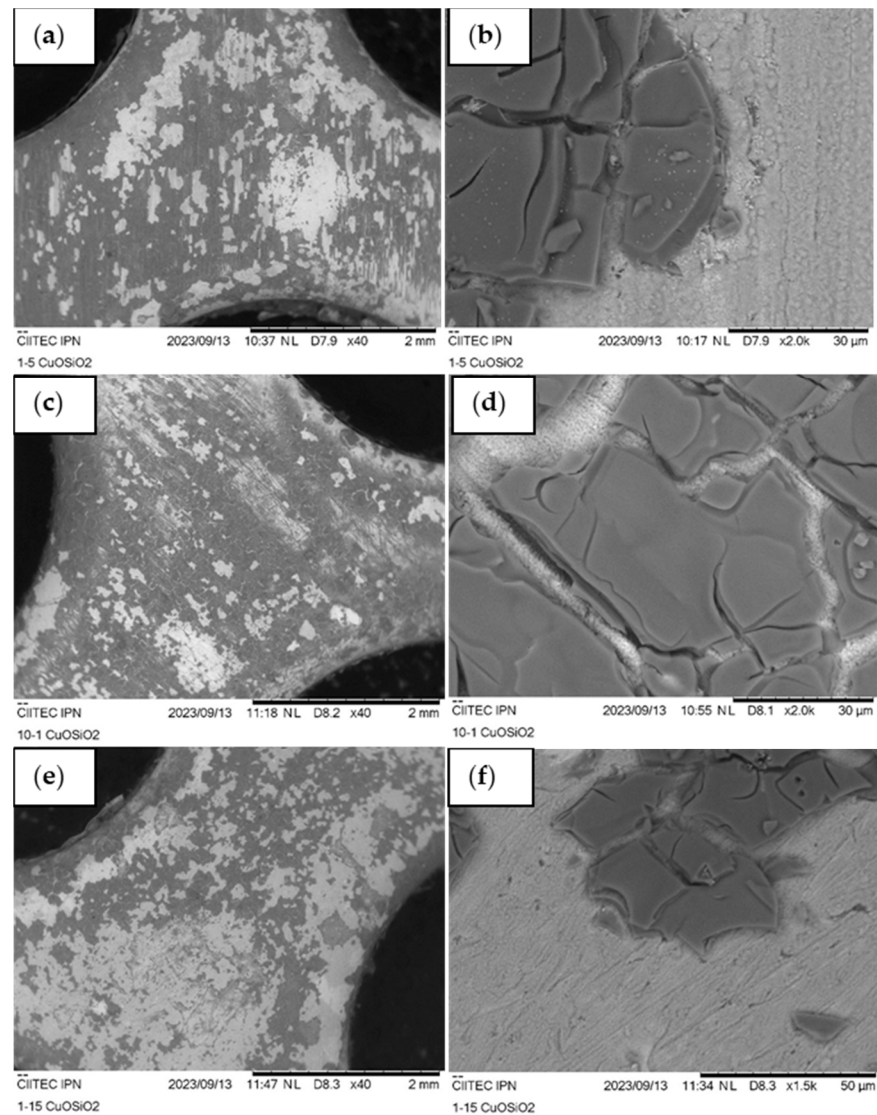


Figure 7. (a) CuO:SiO₂ molar ratio of 1:5 at 40× magnification and (b) 1:5 molar ratio at 2000× magnification. (c) CuO:SiO₂ molar ratio of 1:10 at 40× magnification and (d) 1:10 molar ratio at 2000× magnification. (e) CuO:SiO₂ molar ratio of 1:15 at 40× magnification and (f) 1:15 molar ratio at 1500× magnification.

Depending on the heating ramp, the SiO₂ framework may compact more or less due to the solvent liberation rate [42]. In contrast, in the case of the CuO/SiO₂ sol viscosity, this effect affects the thickness of the deposited layer, as the species concentration is increased and results in a higher dragging level from the steel substrate when dip-coating immersion is performed [43].

In the micrographs for the 1:10 molar ratio at 40× magnification (Figure 7c), the same film cracks provoked by the thermal treatments can be observed. From the micrographs, it can be suggested that the deposits had better adherence with an intermediate Cu loading in SiO₂ due to the suitable equilibrium between the CuO-SiO₂ and CuO/SiO₂ steel interfaces. This effect can also be observed at 2000× magnification (Figure 7d), as the flakes are visibly more uniform.

In the micrograph corresponding to the 1:15 molar ratio at 40× magnification (Figure 7e), a larger gray-white zone is evident, which indicates a decrease in the deposition amount of the CuO/SiO₂ system. Likewise, the formation of cracked-flake-shaped structures can be seen at 1500× magnification (Figure 7f). It is possible that a lower CuO load could cause the weakening of the anchoring of the CuO/SiO₂ system on the steel substrate. The

analysis using energy dispersive spectroscopy (EDS) of the sample with the 1:10 molar ratio at 2000× magnification (Figure 8) was carried out.

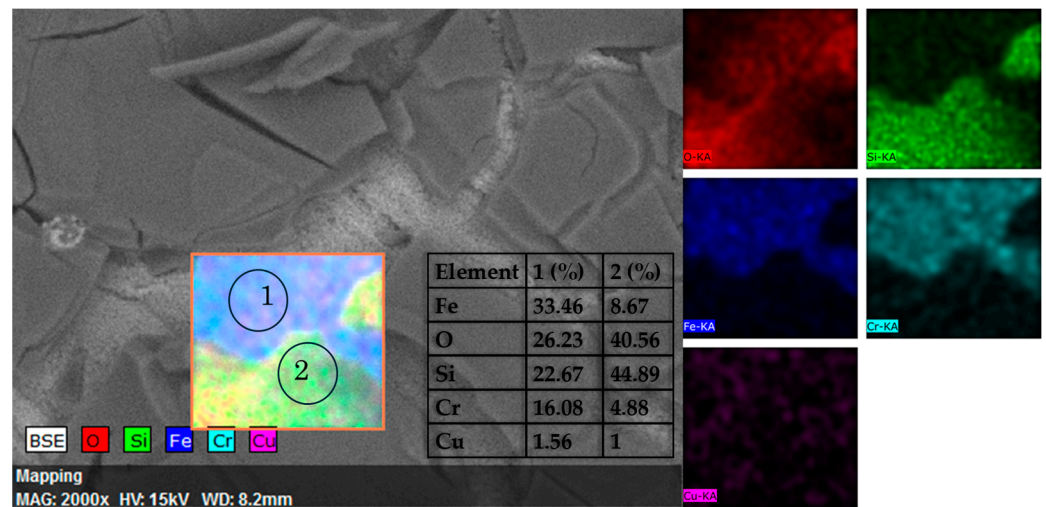


Figure 8. EDS analysis of a micrograph at 2000× magnification of the CuO/SiO₂ system films for the 1:10 molar ratio. The percentages correspond to two mapped areas, delimited by a circle, named zones 1 and 2, respectively.

The presence of Cu and Si was verified in a light-gray zone marked with number 1 and with 1.56 wt.% and 22.67 wt.%, respectively, thus evidencing zones with higher deposited amounts of the CuO/SiO₂ system. The SiO₂ matrix is deposited to a higher extent in zone 2 with 44.89 wt.%, which indicates that zone 2, showing cracked flakes, concentrates more abundant cumuli of SiO₂. The Fe and Cr percentages correspond to the 304 stainless steel substrates. The weight percent increase of Si from zone 1 to zone 2 from 22.67 wt.% to 44.89 wt.%(values in Figure 8) reveals the concentration growth of the CuO/SiO₂ system deposited in zone 2. The decrease in the Cu percentage from zone 1 to zone 2, from 1.56 wt.% to 1 wt.%, respectively, could have been due to the fact that the particles were embedded to a higher amount in SiO₂, thus resulting in less presence of CuO on the surface of the sampled zone.

To support this assertion, the surface of the 304 stainless steel substrate was analyzed. Figure 9a shows the micrograph before depositing the CuO/SiO₂ system.

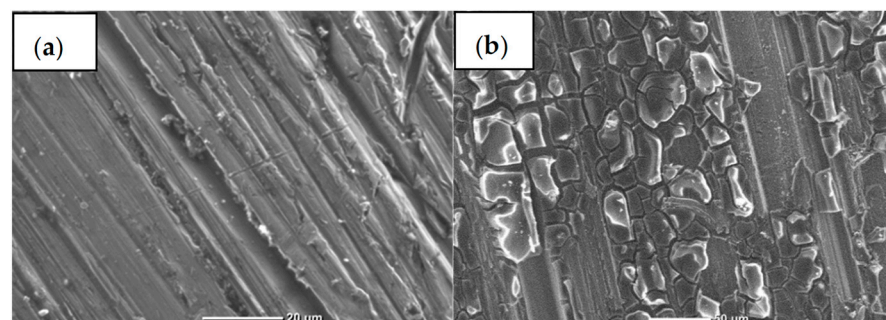


Figure 9. (a) Micrograph of the 304 stainless steel substrate without coating at 1100× magnification and (b) 304 stainless steel substrate at 340× magnification after the dip-coating deposition process of the CuO/SiO₂ system. The micrograph was taken after subjecting the substrate to a MB degradation process for 1500 min.

The steel surface was subjected to an abrading process, which produced micro-metric irregularities. This treatment created anchoring sites for better adherence of the deposited material.

Figure 9b displays a micrograph taken at 350 \times magnification of a section of the CuO/SiO₂ system film for the 1:10 molar ratio after performing the degradation process of MB for 1500 min. The incrustation of the system can be observed in most of the sampled areas of the 304 stainless steel substrates. The material anchorage can be seen in the metal concavities, even after 1500 min of a continuous process subject to stirring and bubbling.

3.3. Photocatalytic Evaluation of CuO and CuO/SiO₂

3.3.1. Methylene Blue (MB)

During the assay carried out with the CuO powders (Figure 10a), the first test confirmed the degradation efficiency (10%) solely by employing light, which could have been promoted through oxidative processes (featuring environmental oxygen) activated by the energy contribution supplied from 4.5 W conventional lamps. Afterward, it is observed that the MB:CuO molar ratio of 1:1 displays a similar trend to that of the photolysis study. It is possible that the lower amount of active CuO sites was not enough to evidence a considerable concentration reduction of MB during the 200 min assay [44].

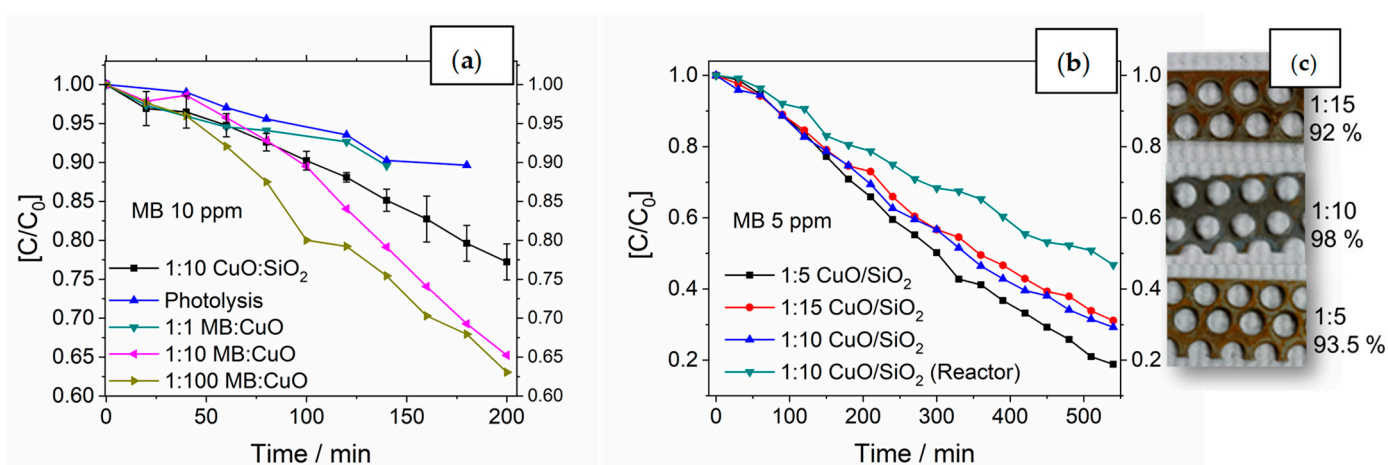


Figure 10. (a) Study of the concentration effect of the CuO powders on the degradation of MB and with the CuO/SiO₂ system at the molar ratio of 1:10. (b) Degradation assays of MB at three molar ratios of the CuO/SiO₂ system films and with the 10.7 cm substrates in the aerated and stirred tank reactor. (c) Photograph of the substrates after 1500 min of treatment and maximal efficiencies.

In the curve of the MB:CuO molar ratio of 1:10, the efficiency increased from 10% to 35%. The amount of particles was enough to start the photodegradation processes, thus augmenting the presence of \bullet OH radicals. With the MB:CuO molar ratio of 1:100, an increase of 3% with respect to the previous ratio (1:10) can be observed; this increment is not significant enough because the CuO amount was 10 times greater and the achieved photodegradation percentage was just 3%. This fact is because a CuO-dispersed solution darkens the medium at higher concentrations, thus participating in the reception of photons by the photocatalyst. The MB:CuO molar ratios of 1:10 and 1:100 display very close efficiencies, which evidences the lower practical efficiency of the powders in the degradation process of water contaminants. MB degradation efficiencies of up to 60% have been reported with the use of CuO powders at 100 min [45]. However, the results are not completely comparable due to variations in the power of the lamps, which have reported irradiance values above 800 W/m². Comparisons such as those by Ahmad et al. [46] unveil important variations in the light source and photocatalyst.

The test with the films of the CuO/SiO₂ system, under the same conditions (indicated in black in Figure 10a), achieved a 25% efficiency in degrading MB at 10 ppm. A decrease in the removal percentage is expected because, in immobilized systems, there is less available photocatalyst interfacial area [47]. It is also worth considering that the amount of CuO dispersed in the SiO₂ film is lower than that of the material deposited directly in the MB solution. However, the accomplished efficiency can still be considered good, as it is just

10% lower than the one obtained with the MB:CuO molar ratio of 1:10. The main advantage is that the immobilized system does not feature the drawback of solution particles that produce an opaque medium. Furthermore, it is possible to increase the number of substrates to enhance the degradation rate of contaminants, and no secondary stages are necessary for the separation of the active material.

Figure 10b shows the degradation curves of MB at 5 ppm with the CuO/SiO₂ system films. The concentration reduction was carried out to track the degradation level more accurately over shorter periods. Studying the three molar ratios helps in selecting the most suitable ratio for evaluation in the reactor. Apparently, the molar ratio of 1:5, which has the highest CuO loading, achieves a higher degradation percentage during the 540 min of exposure to visible light (81%). The 1:10 molar ratio, with half of the CuO load, experiences only a 10% reduction in efficiency, with a degradation percentage of 70%. For the molar ratio of 1:15, the percentage of degradation is similar to that achieved with the 1:10 ratio.

Additionally, 1.5 × 5 cm 304 stainless steel substrates coated with the CuO/SiO₂ system were subjected to continuous treatment of MB degradation for 1500 min. The maximal degradation efficiencies accomplished using the systems at 1:5, 1:10, and 1:15 molar ratios were 91.95%, 98.25%, and 93.53%, respectively. After 1500 min, the process was stopped, and a color change was observed on the surface of the steel substrates coated with the CuO/SiO₂ system (Figure 10c), transitioning from gray to orange-brown, which can be associated with film detachment and the formation of FeO on the steel substrate due to constant exposure to the aqueous medium. The intermediate load of CuO in SiO₂ shows a less visible color change and the highest removal amount of MB at 1500 min. It is possible that for this molar ratio, the detachment of the CuO/SiO₂ film did not occur. This fact could also explain the higher degradation percentage, considering that there is a higher number of active sites preserved during the whole 1500 min process. Through the SEM study of the CuO/SiO₂ system films, it was observed that for the 1:10 molar ratio (Figure 7c,d), more homogeneous and abundant deposits occur than with the molar ratios of 1:5 (Figure 7a,b) and 1:15 (Figure 7e,f).

The degradation rate could also have been affected by the hydrophobic and hydrophilic character of SiO₂ [31,48]. The uniformity of the deposited SiO₂, as observed in the micrographs displayed in Figure 7, could have created hydrophobic surfaces, potentially reducing the interactions with the support active sites. In addition, the growing SiO₂ concentration increased the probability of this effect, which could happen from the 1:10 molar ratio. Indeed, this negative effect could end up being beneficial for the protection of the steel substrate, for SiO₂ has been employed as an anticorrosion barrier in different metals [49–51]. Additionally, the formation of copper silicates has a positive effect on the photocatalytic properties of the CuO/SiO₂ system. Liming et al. [52] synthesized a photocatalyst featuring the CuO/SiO₂ system using the sol-gel method with 17.8 wt.%, 37.8 wt.%, and 42.2 wt.% loadings of CuO and SiO₂. It was found that the CuO increase promoted the formation of copper silicates finely dispersed on the photocatalyst surface, thus confirming that the catalytic properties of the CuO/SiO₂ system are directly affected by CuO loading.

Finally, the 10.7 cm circular substrates inserted in the reactor and subjected to the degradation process of MB at 5 ppm achieved an efficiency of 53%. The increase in the working volume and different arrangements of the employed elements (bubble generator and stirrer) represent changes that determine the interaction between the photocatalyst and contaminant.

Furthermore, the increase in the recipient radius creates a wider barrier for the penetration of light into the tank volume, thus reducing the homogeneous reception of photons in the whole area of the discs, in addition to the deposit proper factors, such as the dispersion of CuO species in the SiO₂ matrix, which affects the recombination rate of charge carriers of the photocatalyst [53].

3.3.2. Amoxicillin

For the AMX degradation assays, firstly, 1.5×5 cm substrates were employed, and then, the test with the steel discs at the optimal CuO:SiO₂ molar ratio of 1:10 was carried out in the aerated and stirred tank reactor. Figure 11 shows the degradation curves of AMX for the two tests.

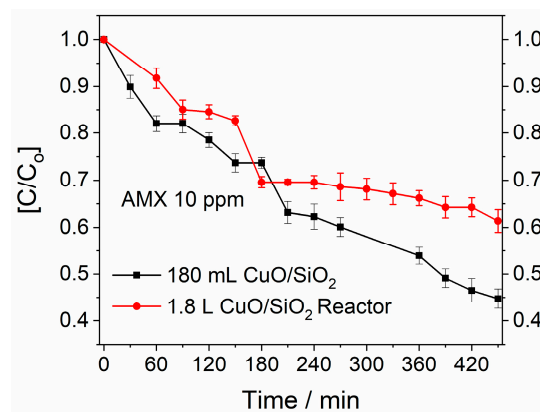


Figure 11. Degradation curves of AMX with the CuO/SiO₂ system at a molar ratio of 1:10.

At a volume of 180 mL, the maximal percentage at 450 min is 55.2%, and for the 10.7 cm circular substrates in the reactor, it is 38.6%. These results are in good agreement with those obtained in the degradation of MB, as there is an efficiency reduction with the increasing working volume. The photocatalytic process requires, first, a sufficient amount of light, which triggers the generation of hydroxyl and superoxide radicals that ultimately attack the pharmaceutical organic structure, degrading it under ideal conditions to CO₂ and H₂O. These requirements are affected by the complexity and stability of the organic structure. Furthermore, the oxygen supply and need for more powerful stirring can be vital for efficiency at higher volumes [54].

In order to evidence the diminution of the characteristic AMX bands, UV–Vis scanning from 250 to 800 nm was carried out (Figure 12). Three samples were taken at 0, 300, and 1500 min of the degradation assay in 180 mL. The band at 270 nm, characteristic of AMX, presents a gradual reduction throughout the assay, which is in good agreement with the degradation curve in Figure 12; specifically, from 30 min, a wide band corresponding to the AMX degradation products occurs.

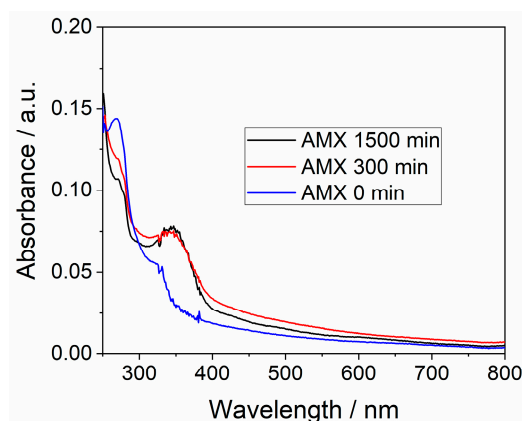


Figure 12. Whole scanning from 200 to 800 nm at 3 different degradation times.

Every part of the photocatalytic system plays an important role in the degradation process of the mentioned organic structures. The incorporation of mechanical stirring and upward bubbling enables the improvement of the photocatalyst reaction conditions employing the model molecules (MB and AMX). The photocatalyst embedded in the matrix

was deposited on perforated steel discs to allow its introduction into the reactor and avoid subsequent separation stages. Finally, a photodegradation study was carried out with pure CuO powders, varying the CuO load on SiO₂ films, and with the whole CuO/SiO₂ system in the reactor. Four 4.5 W lamps were used in both processes; for the reactor, a 100 W lamp was added, approximating the increase in power with the increase in volume. The equivalence factor of 10 corresponds to 180 W for the 18 W supplied by the four 4.5-W lamps. Then, the overall sum of the reactor power was 118 W, which implies a reduction of 35%. Therefore, the reduction in efficiency is also linked to the lower supplied power. A series of stages is necessary, which involves obtaining the photocatalyst powders, making the films, building the reactor, and finally performing the photocatalytic evaluation.

The synergistic action occurring between the CuO/SiO₂/water solution and UV irradiation forms the OH radicals, biradicals, and O₂⁻ ion radicals, where every set contributes to AMX degradation (Figure 13). Initially, the complex AMX structure suffers a gradual rupture, where the penicilloic and penilloic acids have been identified by different authors [55]. Finally, the sulfate and ammonium ions result from the complete fragmentation of AMX. The thorough mineralization process yields CO₂ and H₂O as final products [56], achieving efficient photocatalytic degradation.

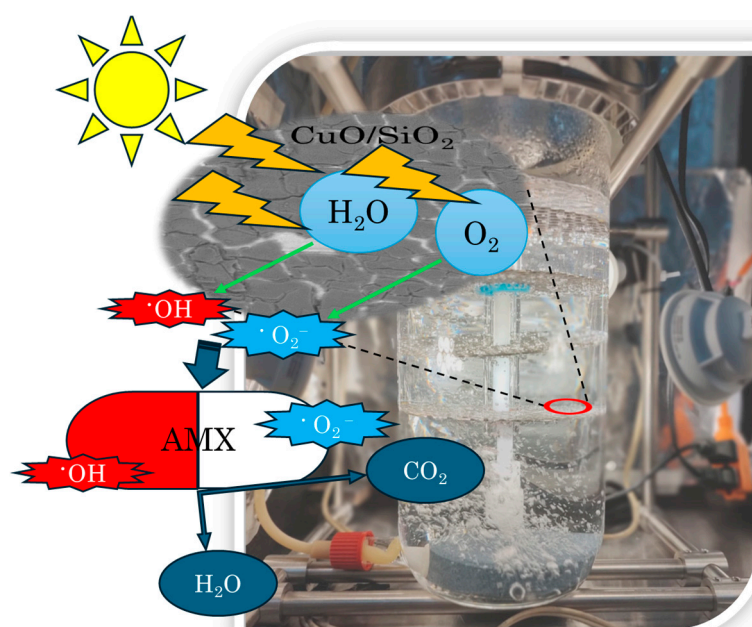


Figure 13. AMX degradation via synergistic action.

4. Conclusions

CuO powders were synthesized with monoclinic structures, polyhedral morphology, size distributions between 0.5 and 2.5 μm (with an average of $1.26 \pm 0.07 \mu\text{m}$), and an Eg of 1.8 eV, estimated using the graphical Tauc method. CuO/SiO₂ films were deposited on steel substrates at CuO:SiO₂ molar ratios of 1:5, 1:10, and 1:15.

The CuO powders were evaluated in volumes of 180 mL at MB:CuO molar ratios of 1:1, 1:10, and 1:100 and at 10 ppm. The photocatalytic efficiencies achieved in 200 min were 10%, 35%, and 37%, respectively. The powder amount interfered with the photocatalytic efficiency derived from the opaqueness increase in the solution with the growing concentration. The CuO/SiO₂ system films were evaluated. The increase in the CuO concentration affected the faster MB degradation rate in 540 min; notwithstanding, the molar ratio of 1:10 proved itself to be the highest degradation efficiency (98%) at 1500 min, with the least significant color change associated with low deposit detachment.

For the AMX degradation, the CuO/SiO₂ system films were evaluated at a molar ratio of 1:10 in two working volumes: 180 mL and 1.8 L (reactor). The achieved efficiencies at 450 min were 55% and 38%.

A deeper understanding of all the phenomena implied in the efficiency of the deposited photocatalysts will allow the solution of the problematic scaling of these processes. The production of a synergistic effect involving suitable efficiency, low cost, and design practicality seems to be the challenge to overcome when using heterogeneous photocatalysis in the treatment of wastewater at the plant level.

Author Contributions: Conceptualization, A.G.-H. and I.V.L.; methodology, A.H.-R. and C.H.-F.; software, C.H.-F.; validation, I.V.L. and N.V.L.; formal analysis, E.Y.C.-M.; investigation, A.H.-R.; resources, Á.d.J.M.-R. and O.O.-X.; writing—A.H.-R.; writing—review and editing, I.V.L. and N.V.L.; visualization, A.G.-H.; supervision, I.V.L.; project administration, I.V.L.; funding acquisition, A.H.-R. All authors have read and agreed to the published version of the manuscript.

Funding: The authors are grateful to CONACYT for the scholarship granted to pursue postgraduate studies (Alberto Hernandez-Reyes) and to SIP-IPN (Proyecto 20241750) for their financial support.

Institutional Review Board Statement: “Not applicable” for studies not involving humans or animals.

Informed Consent Statement: “Not applicable” for studies not involving humans or animals.

Data Availability Statement: Data are contained within the article.

Conflicts of Interest: The authors declare no conflicts of interest.

References

1. López-Pacheco, I.Y.; Silva-Núñez, A.; Salinas-Salazar, C.; Arévalo-Gallegos, A.; Lizarazo-Holguin, L.A.; Barceló, D.; Iqbal, H.M.N.; Parra-Saldívar, R. Anthropogenic contaminants of high concern: Existence in water resources and their adverse effects. *Sci. Total Environ.* **2019**, *690*, 1068–1088. [[CrossRef](#)] [[PubMed](#)]
2. Shehu, Z.; Nyakairu, G.W.A.; Tebandeke, E.; Odume, O.N. Overview of African water resources contamination by contaminants of emerging concern. *Sci. Total Environ.* **2022**, *852*, 158303. [[CrossRef](#)] [[PubMed](#)]
3. Zhu, S.; Chen, H.; Li, J. Sources, distribution and potential risks of pharmaceuticals and personal care products in Qingshan Lake basin, Eastern China. *Ecotoxicol. Environ. Saf.* **2013**, *96*, 154–159. [[CrossRef](#)] [[PubMed](#)]
4. Pico, Y.; Belenguer, V.; Corcellas, C.; Diaz-Cruz, M.S.; Eljarrat, E.; Farré, M.; Gago-Ferrero, P.; Huerta, B.; Navarro-Ortega, A.; Petrovic, M.; et al. Contaminants of emerging concern in freshwater fish from four Spanish Rivers. *Sci. Total Environ.* **2019**, *659*, 1186–1198. [[CrossRef](#)] [[PubMed](#)]
5. Sierra, E.M.; Gálvez, E.M.; Mendoza, I.A.G.; Mendoza, M.D.G.; Galvéz, M.B. *Manejo Práctico de los Antibióticos: Farmacología, Indicaciones y Dosis en Pacientes Adultos y Pediátricos*; Edición Kindle; 2016.
6. Oladoye, P.O.; Ajiboye, T.O.; Omotola, E.O.; Oyewola, O.J. Methylene blue dye: Toxicity and potential elimination technology from wastewater. *Results Eng.* **2022**, *16*, 100678. [[CrossRef](#)]
7. Lorenzo, P.; Adriana, A.; Jessica, S.; Carles, B.; Marinella, F.; Marta, L.; Luis, B.J.; Pierre, S. Antibiotic resistance in urban and hospital wastewaters and their impact on a receiving freshwater ecosystem. *Chemosphere* **2018**, *206*, 70–82. [[CrossRef](#)] [[PubMed](#)]
8. Li, X.; Lin, L.; Liu, Z.; Yang, J.; Ma, W.; Yang, X.; Li, X.; Wang, C.; Xin, Q.; Zhao, K. A “micro-explosion” strategy for preparing membranes with high porosity, permeability, and dye/salt separation efficiency. *J. Ind. Eng. Chem.* **2023**, *119*, 516–531. [[CrossRef](#)]
9. Fonseca Couto, C.; Lange, L.C.; Santos Amaral, M.C. A critical review on membrane separation processes applied to remove pharmaceutically active compounds from water and wastewater. *J. Water Process Eng.* **2018**, *26*, 156–175. [[CrossRef](#)]
10. Vieira, W.T.; de Farias, M.B.; Spaolozzi, M.P.; da Silva, M.G.C.; Vieira, M.G.A. Removal of endocrine disruptors in waters by adsorption, membrane filtration and biodegradation. A review. *Environ. Chem. Lett.* **2020**, *18*, 1113–1143. [[CrossRef](#)]
11. Wang, X.; Sayed, M.; Ruzimuradov, O.; Zhang, J.; Fan, Y.; Li, X.; Bai, X.; Low, J. A review of step-scheme photocatalysts. *Appl. Mater. Today* **2022**, *29*, 101609. [[CrossRef](#)]
12. Pourret, O.; Bollinger, J.-C.; Hursthouse, A.; van Hullebusch, E.D. Sorption vs adsorption: The words they are a-changin’, not the phenomena. *Sci. Total Environ.* **2022**, *838*, 156545. [[CrossRef](#)] [[PubMed](#)]
13. Ahmed, M.J.; Hameed, B.H. Removal of emerging pharmaceutical contaminants by adsorption in a fixed-bed column: A review. *Ecotoxicol. Environ. Saf.* **2018**, *149*, 257–266. [[CrossRef](#)] [[PubMed](#)]
14. Li, N.; Yan, X.; Dai, W.; Lv, B.; Wang, W. Adsorption Properties and Mechanism of Sepiolite to Graphene Oxide in Aqueous Solution. *Arab. J. Chem.* **2023**, *16*, 104595. [[CrossRef](#)]
15. Wu, X.; Zhang, J.; Hu, S.; Zhang, G.; Lan, H.; Peng, J.; Liu, H. Evaluation of degradation performance toward antiviral drug ribavirin using advanced oxidation process and its relations to ecotoxicity evolution. *Sci. Total Environ.* **2022**, *850*, 157851. [[CrossRef](#)] [[PubMed](#)]

16. Meropoulis, S.; Giannoulia, S.; Skandalis, S.; Rassias, G.; Aggelopoulos, C.A. Key-study on plasma-induced degradation of cephalosporins in water: Process optimization, assessment of degradation mechanisms and residual toxicity. *Sep. Purif. Technol.* **2022**, *298*, 121639. [[CrossRef](#)]
17. Jin, D.; Lv, Y.; He, D.; Zhang, D.; Liu, Y.; Zhang, T.; Cheng, F.; Zhang, Y.; Sun, J.; Qu, J. Photocatalytic degradation of COVID-19 related drug arbidol hydrochloride by Ti3C2 MXene/supramolecular g-C₃N₄ Schottky junction photocatalyst. *Chemosphere* **2022**, *308*, 136461. [[CrossRef](#)] [[PubMed](#)]
18. Silva, T.L.; da Costa, C.S.D.; Silva, M.G.C.d.; Vieira, M.G.A. Overview of non-steroidal anti-inflammatory drugs degradation by advanced oxidation processes. *J. Clean. Prod.* **2022**, *346*, 131226. [[CrossRef](#)]
19. Thanh Tung, M.H.; Thu Phuong, T.T.; Phuong Le Chi, N.T.; The, D.M.; Quoc, N.T.; Khan, D.T.; Pham, T.-D.; Khoa, N.V.; Thu Hien, T.T.; Dieu Cam, N.T. Novel amoxicillin degradation via photocatalysis of WO₃/AgI heterojunction decorated on rGO. *Ceram. Int.* **2023**, *49*, 10881–10888. [[CrossRef](#)]
20. Yahia, B.; Faouzi, S.; Ahmed, C.; Lounis, S.; Mohamed, T. A new hybrid process for Amoxicillin elimination by combination of adsorption and photocatalysis on (CuO/AC) under solar irradiation. *J. Mol. Struct.* **2022**, *1261*, 132769. [[CrossRef](#)]
21. Jeyarani, W.J.; Tenkyong, T.; Bachan, N.; Kumar, D.A.; Shyla, J.M. An investigation on the tuning effect of glucose-capping on the size and bandgap of CuO nanoparticles. *Adv. Powder Technol.* **2016**, *27*, 338–346. [[CrossRef](#)]
22. Ahmad, I.; Shukrullah, S.; Naz, M.Y.; Ahmed, E.; Ahmad, M.; Akhtar, M.S.; Ullah, S.; Farooq, M.U.; Iqbal, S.; Assiri, M.A.; et al. Microwave-assisted one-pot hydrothermal synthesis of V and La co-doped ZnO/CNTs nanocomposite for boosted photocatalytic hydrogen production. *Int. J. Hydrogen Energy* **2022**, *47*, 15505–15515. [[CrossRef](#)]
23. Bao, X.; Lv, X.; Wang, Z.; Wang, M.; Liu, M.; Dai, D.; Zheng, L.; Zheng, Z.; Cheng, H.; Wang, P.; et al. Nitrogen vacancy enhanced photocatalytic selective oxidation of benzyl alcohol in g-C₃N₄. *Int. J. Hydrogen Energy* **2021**, *46*, 37782–37791. [[CrossRef](#)]
24. Bahadoran, A.; Masudy-Panah, S.; De Lile, J.R.; Li, J.; Gu, J.; Sadeghi, B.; Ramakrishna, S.; Liu, Q. Novel 0D/1D ZnBi₂O₄/ZnO S-scheme photocatalyst for hydrogen production and BPA removal. *Int. J. Hydrogen Energy* **2021**, *46*, 24094–24106. [[CrossRef](#)]
25. Yu, Q.; Ma, X.; Wang, M.; Yu, C.; Bai, T. Influence of embedded particles on microstructure, corrosion resistance and thermal conductivity of CuO/SiO₂ and NiO/SiO₂ nanocomposite coatings. *Appl. Surf. Sci.* **2008**, *254*, 5089–5094. [[CrossRef](#)]
26. Venkadesh, A.; Mathiyarasu, J.; Radhakrishnan, S. A highly uniform CuO@SiO₂ porous sphere with improved electrochemical sensing performance for the accurate determination of vanillin in food samples. *Mater. Today Chem.* **2021**, *22*, 100554. [[CrossRef](#)]
27. Zarzuela, R.; Almoraima Gil, M.L.; Carretero, J.; Carbú, M.; Cantoral, J.M.; Mosquera, M.J. Development of a novel engineered stone containing a CuO/SiO₂ nanocomposite matrix with biocidal properties. *Constr. Build. Mater.* **2021**, *303*, 124459. [[CrossRef](#)]
28. Sharma, S.; Basu, S. Construction of an efficient and durable hierarchical porous CuO/SiO₂ monolith for synergistically boosting the visible-light-driven degradation of organic pollutants. *Sep. Purif. Technol.* **2021**, *279*, 119759. [[CrossRef](#)]
29. Nogueira, A.C.; Gomes, L.E.; Ferencz, J.A.P.; Rodrigues, J.E.F.S.; Gonçalves, R.V.; Wender, H. Improved Visible Light Photoactivity of CuBi₂O₄/CuO Heterojunctions for Photodegradation of Methylene Blue and Metronidazole. *J. Phys. Chem. C* **2019**, *123*, 25680–25690. [[CrossRef](#)]
30. Latif, A.; Memon, A.M.; Gadhi, T.A.; Bhurt, I.A.; Channa, N.; Mahar, R.B.; Ali, I.; Chiadò, A.; Bonelli, B. Bi₂O₃ immobilized 3D structured clay filters for solar photocatalytic treatment of wastewater from batch to scaleup reactors. *Mater. Chem. Phys.* **2022**, *276*, 125297. [[CrossRef](#)]
31. Wang, Y.; Liu, C.; Li, Y.; Fan, T.; Wu, Z. A facile construction strategy of SiO₂-modified anodic film on 304 stainless steel by introducing TEOS into fluoride-based ethylene glycol electrolyte. *Mater. Today Commun.* **2023**, *36*, 106711. [[CrossRef](#)]
32. Subasri, R.; Malathi, R.; Jyothirmayi, A.; Hebalkar, N.Y. Synthesis and characterization of CuO-hybrid silica nanocomposite coatings on SS 304. *Ceram. Int.* **2012**, *38*, 5731–5740. [[CrossRef](#)]
33. Arige, S.; Mishra, V.; Miryala, M.; Rao, M.S.R.; Dixit, T. Plasmon-coupled sub-bandgap photoluminescence enhancement in ultra-wide bandgap CuO through hot-hole transfer. *Opt. Mater.* **2022**, *134*, 113149. [[CrossRef](#)]
34. Hanif, M.A.; Lee, I.; Akter, J.; Islam, M.A.; Zahid, A.A.S.M.; Sapkota, K.P.; Hahn, J.R. Enhanced Photocatalytic and Antibacterial Performance of ZnO Nanoparticles Prepared by an Efficient Thermolysis Method. *Catalysts* **2019**, *9*, 608. [[CrossRef](#)]
35. Chen, Y.-W.; Chen, Y.-S.; Lin, S.-F.; Chen, Y.-Y.; Hung, W.-Y.; Lin, H.-P.; Tang, C.-Y.; Lin, C.-Y.; Hsu, C.-H. Transformation of Cu(OH)₂ to mesostructural copper-silicate in alkaline silicate solution. *Mater. Today Sustain.* **2023**, *24*, 100535. [[CrossRef](#)]
36. Cao, G.; Guo, M.; Yang, F.; Xu, H.; Shao, G.; Hu, J. The effect of nanometre-scale kinetic competition on the phase selection in Zr/Si superstructure. *Mater. Charact.* **2024**, *208*, 113666. [[CrossRef](#)]
37. Cao, G.; Chen, C.; Xu, H.; Ban, J.; Liu, F.; Yuan, G.; Lei, H.; Su, Y.; Hu, J. Chemical regulation in the bonding reconstruction stage of amorphous Zr-Si oxidation and the resultant phase selection. *Mater. Des.* **2023**, *233*, 112291. [[CrossRef](#)]
38. Shi, B.; Xie, L.; Ma, B.; Zhou, Z.; Xu, B.; Qu, L. Preparation and Properties of Highly Transparent SiO₂ Aerogels for Thermal Insulation. *Gels* **2022**, *8*, 744. [[CrossRef](#)] [[PubMed](#)]
39. Zawada, A.; Lubas, M.; Przerada, I. Application of Mössbauer spectroscopy and FT-IR to describe coordination of amphoteric ions in structure of glasses from the SiO₂-Na₂O-MgO-CaO-Al₂O₃-Fe₂O₃ system. *J. Mol. Struct.* **2023**, *1285*, 135368. [[CrossRef](#)]
40. Akter, J.; Sapkota, K.P.; Hanif, M.A.; Islam, M.A.; Abbas, H.G.; Hahn, J.R. Kinetically controlled selective synthesis of Cu₂O and CuO nanoparticles toward enhanced degradation of methylene blue using ultraviolet and sun light. *Mater. Sci. Semicond. Process.* **2021**, *123*, 105570. [[CrossRef](#)]
41. Raul, P.K.; Senapati, S.; Sahoo, A.K.; Umlong, I.M.; Devi, R.R.; Thakur, A.J.; Veer, V. CuO nanorods: A potential and efficient adsorbent in water purification. *RSC Adv.* **2014**, *4*, 40580–40587. [[CrossRef](#)]

42. Mohan, M.; Thangavel, K.; Balaprakash, V. Characterization of CZO thin films prepared by Sol-Gel dip coating technique with varied concentrations and annealed at different temperatures. *Chem. Phys.* **2023**, *573*, 111981. [[CrossRef](#)]
43. Mohd Yusoff, M.F.; Abdul Kadir, M.R.; Iqbal, N.; Hassan, M.A.; Hussain, R. Dipcoating of poly (ϵ -caprolactone)/hydroxyapatite composite coating on Ti6Al4V for enhanced corrosion protection. *Surf. Coat. Technol.* **2014**, *245*, 102–107. [[CrossRef](#)]
44. Patil, D.; Manjanna, J.; Chikkamath, S.; Uppar, V.; Chougala, M. Facile synthesis of stable Cu and CuO particles for 4-nitrophenol reduction, methylene blue photodegradation and antibacterial activity. *J. Hazard. Mater. Adv.* **2021**, *4*, 100032. [[CrossRef](#)]
45. Riaz, R.; Bibi, I.; Majid, F.; Kamal, S.; Al Huwayz, M.; Jilani, K.; Ghafoor, A.; Raza, Q.; Alwadai, N.; Iqbal, M. NiFe₂O₄/CuO heterostructures optical, magnetic and photocatalytic properties: Methylene blue dye degradation under solar light irradiation. *J. Mol. Struct.* **2024**, *1309*, 138174. [[CrossRef](#)]
46. Ahmad, A.; Khan, M.; Khan, S.; Luque, R.; Abualnaja, K.M.; Alduaij, O.K.; Yousef, T.A. Bio-Construction of CuO Nanoparticles Using Texas Sage Plant Extract for catalytical degradation of Methylene blue Via Photocatalysis. *J. Mol. Struct.* **2022**, *1256*, 132522. [[CrossRef](#)]
47. Manassero, A.; Satuf, M.L.; Alfano, O.M. Photocatalytic reactors with suspended and immobilized TiO₂: Comparative efficiency evaluation. *Chem. Eng. J.* **2017**, *326*, 29–36. [[CrossRef](#)]
48. Althamthami, M.; Elhachmi, G.T.; Ben Temam, H.; Hasan, G.G.; Rahmane, S.; Gasmi, B. Effect of Different Cu:Co Film Concentrations on Photocatalytic Reactions of Ethanol, MB, AMX, and Cr(VI): A Study of Film Properties & Effects of Photooxidation. *J. Environ. Chem. Eng.* **2023**, *11*, 111247. [[CrossRef](#)]
49. Zhang, X.-F.; Li, X.-D.; Wang, N.; Liu, Y.-J.; Tian, F.; Wang, C.-X. Robust superhydrophobic SiO₂/epoxy composite coating prepared by one-step spraying method for corrosion protection of aluminum alloy: Experimental and theoretical studies. *Mater. Des.* **2023**, *228*, 111833. [[CrossRef](#)]
50. Xijing, L.; Yong, C. Effect of SiO₂ nanoparticles on the hardness and corrosion resistance of NiW/SiO₂ nano composite coating prepared by electrodeposition. *Int. J. Electrochem. Sci.* **2023**, *18*, 100138. [[CrossRef](#)]
51. Zhang, T.; Zhang, Y.; Chen, C.; Tian, Y.; Wang, Y.; Cao, S.; Ma, J. Corrosion-resistant SiO₂-graphene oxide/epoxy coating reinforced by effective electron beam curing. *Prog. Org. Coat.* **2023**, *184*, 107855. [[CrossRef](#)]
52. He, L.; Chen, X.; Ma, J.; He, H.; Wang, W. Characterization and catalytic performance of sol-gel derived Cu/SiO₂ catalysts for hydrogenolysis of diethyl oxalate to ethylene glycol. *J. Sol-Gel Sci. Technol.* **2010**, *55*, 285–292. [[CrossRef](#)]
53. Vezzoli, M.; Farrell, T.; Baker, A.; Psaltis, S.; Martens, W.N.; Bell, J.M. Optimal catalyst thickness in titanium dioxide fixed film reactors: Mathematical modelling and experimental validation. *Chem. Eng. J.* **2013**, *234*, 57–65. [[CrossRef](#)]
54. Tapia-tlatelpa, T.; Buscio, V.; Trull, J.; Sala, V. Performance analysis and methodology for replacing conventional lamps by optimized LED arrays for photocatalytic processes. *Chem. Eng. Res. Des.* **2020**, *156*, 456–468. [[CrossRef](#)]
55. Aksu Demirezen, D.; Yıldız, Y.Ş.; Demirezen Yılmaz, D. Amoxicillin degradation using green synthesized iron oxide nanoparticles: Kinetics and mechanism analysis. *Environ. Nanotechnol. Monit. Manag.* **2019**, *11*, 100219. [[CrossRef](#)]
56. Sun, X.; He, K.; Chen, Z.; Yuan, H.; Guo, F.; Shi, W. Construction of visible-light-response photocatalysis-self-Fenton system for the efficient degradation of amoxicillin based on industrial waste red mud/CdS S-scheme heterojunction. *Sep. Purif. Technol.* **2023**, *324*, 124600. [[CrossRef](#)]

Disclaimer/Publisher’s Note: The statements, opinions and data contained in all publications are solely those of the individual author(s) and contributor(s) and not of MDPI and/or the editor(s). MDPI and/or the editor(s) disclaim responsibility for any injury to people or property resulting from any ideas, methods, instructions or products referred to in the content.